GA–A26770

GLOBAL PARTICLE BALANCE MEASUREMENTS IN DIII-D H-MODE DISCHARGES

by
E.A. UNTERBERG, S.L. ALLEN, N.H. BROOKS, T.E. EVANS,
A.W. LEONARD, A.G. McLEAN, J.G. WATKINS, and D.G. Whyte

JULY 2010

GENERAL ATOMICS

DISCLAIMER

GA–A26770

GLOBAL PARTICLE BALANCE MEASUREMENTS IN DIII-D H-MODE DISCHARGES

by
E.A. UNTERBERG,* S.L. ALLEN,† N.H. BROOKS, T.E. EVANS,
A.W. LEONARD, A.G. McLEAN,* J.G. WATKINS‡, and D.G. Whyte¶

This is a preprint of a paper to be presented at the Nineteenth International Conference on Plasma Surface Interactions, May 24-28, 2010, in San Diego, California, and to be published in the *Proceedings.*

*Oak Ridge National Laboratory, Oak Ridge, Tennessee.
†Lawrence Livermore National Laboratory, Livermore, California.
‡Sandia National Laboratories, Albuquerque, New Mexico.
¶Massachusetts Institute of Technology, Cambridge, Massachusetts.

Work supported by
the U.S. Department of Energy under
DE-AC05-00OR22725, DE-AC52-07NA27344,
DE-FC02-04ER54698, DE-AC04-94AL85000,
and DE-FG02-04ER54762

GENERAL ATOMICS PROJECT 30200
JULY 2010

GENERAL ATOMICS

ABSTRACT

Experiments are performed on the DIII-D tokamak to determine the retention rate in an all graphite first-wall tokamak. A time-dependent particle balance analysis shows a majority of the fuel retention occurs during the initial Ohmic and L-mode phase of discharges, with peak fuel retention rates typically $\sim 2 \quad 10^{21}$ D/s. The retention rate can be zero within the experimental uncertainties ($< 3 \quad 10^{20}$ D/s) during the later stationary phase of the discharge. In general, the retention *inventory* can decrease in the stationary phase by $\sim 20 \quad 30\%$ from the initial start-up phase of the discharge. Particle inventories determined as a function of time in the discharge, using a "dynamic" particle balance analysis, agree with more accurate particle inventories directly measured after the discharge, termed "static" particle balance. Similarly, low stationary retention rates are found in discharges with heating from neutral-beams, which injects particles, and from electron cyclotron waves, which does not inject particles. Detailed analysis of the static and dynamic balance methods provide an estimate of the DIII-D global co-deposition rate of $\leq 0.6 - 1.2 \times 10^{20}$ D/s. Dynamic particle balance is also performed on discharges with resonant magnetic perturbation ELM suppression and shows no additional retention during the ELM-suppressed phase of the discharge.

I. INTRODUCTION

Fuel retention, specifically hydrogenic isotope retention, in the plasma facing components (PFCs) of magnetic fusion plasma experiments is a research topic of interest mainly due to the potential for semi-permanent trapping of these isotopes in the PFC material. Retention mechanisms have been determined that can either saturate at some level, i.e. the retention stops increasing with discharge time, or that continue to increase within the discharge time without saturation [1-4]. In future long-pulse burning plasma experiments, e.g. ITER, the retention due to non-saturating mechanisms is of most concern due to the regulatory issues of in-vessel tritium. To date, most fuel retention studies in tokamaks have been carried out with carbon PFCs and thus give an extensive database for cross machine comparisons of retention mechanisms [5-8]. Metal PFC retention studies in tokamaks have been done and find large differences in the details of the permanent trapping mechanisms, but this topic is beyond the scope of this work; see Ref. [9,10].

Fuel retention due to plasma wall interactions in carbon are classified into four characteristic processes; absorption, bulk diffusion, implantation, and co-deposition. Absorption into the carbon porosity saturates quickly every discharge but also outgases after each discharge and is therefore not a concern for fuel retention [4]. Similarly, bulk diffusion of hydrogenic species into graphite is of minimal concern due to very low diffusion coefficients under typical tokamak PFC surface temperatures [11]. Implantation is a saturable process that depends on incident particle energy and flux, as well as surface temperature. Implantation in graphite leads to a deuterium, D, fluence $\sim 10^{21}$ D/m^2 within 20 nm of the surface and a deuterium-to-carbon (D/C) concentration ~ 0.4 for surface temperatures $<500°C$ [11]. Co-deposition occurs through the simultaneous deposition/implantation of the D as a carbon layer grows due to net deposition. This process is caused by ions/neutrals eroded from elsewhere in the vessel being net transported to another region. This scrape-off layer (SOL) transport usually leads to carbon layers forming in the divertor region [12]. The D fuel trapped in such layers is not released except at very high surface temperatures ($> 700°C$) or through extraordinary wall conditioning techniques (e.g. thermo-oxidation [13] or disruptive cleaning [14]). This process is of greatest concern for future devices because: a) the layer can grow continuously throughout the discharge thus indefinitely trapping fuel at a continuous rate; and b) the large amount of effort involved in removing the trapped fuel from these layers of increasing depth.

In this paper, we report on a recent study to quantify the fuel retention mechanisms using various global particle balance methods in the all-graphite DIII-D device. Specifically, the total retention due to absorption and implantation is determined directly via the techniques reported here, and a maximum co-deposition level is inferred from the remaining particles. A combination of unique factors in this study set it apart from the past experiments on this topic. First, a global particle balance calculated continuously through the discharge is directly compared with a particle balance method where the exhausted particles from the pumping system are measured after the discharge and compared with the total amount of particles injected. Secondly, a vessel bake to near 350°C after an experiment is preformed in an effort to measure the amount of retained fuel released from non-permanently trapping mechanisms (i.e., not co-deposition). This second bake is intended to start the PFCs with a "clean" surface that does not have what is termed "loosely bound" fuel (i.e., retention due to absorption and/or shallow implantation). After such a bake, by careful measurement, one can then determine the semi-permanent trapped particles; what have been termed "tightly bound" which need extremely high temperature (> 700°C), disruptive cleaning, or thermo-oxidation to be removed. A vessel bake, at 350°C, is also performed before each experiment.

In Sec. II, a detailed description of the within shot particle balance as well as the between shot particle balance is given. Results of these analysis methods are given in Sec. III for a range of plasma conditions, including a series of discharges that had a vessel bake afterwards to record the amount released due to the short-term fuel retention. Sec. IV discusses these results as they relate to past studies of fuel retention in tokamaks. Finally, conclusions are drawn in Sec. V.

II. SETUP AND ANALYSIS TECHNIQUE

In this context, a global particle balance is simply a balance of the vessel sources and sinks during a discharge. Specifically, it calculates the amount of particles injected into the vessel and compares them to the particles that go: into the core plasma; the exhaust system of the vessel; and/or into the carbon PFCs. This balance takes the following familiar form [15-18]:

$$\Gamma_{\mathrm{WALL}}(t) = \Gamma_{\mathrm{IN}}(t) - \left[Q_{\mathrm{PUMP}}(t) + \frac{dN_{\mathrm{P}}(t)}{dt} + \frac{dN_0(t)}{dt} \right] \quad . \tag{1}$$

Here, $\Gamma_{\mathrm{WALL}}(t)$ is a calculation of the particle retention rate (D/s) in vessel tile surfaces and is the remainder of the measured terms on the RHS of Eq. (1). $\Gamma_{\mathrm{IN}}(t)$ is the injected gas rate due to measured gas puffing and/or particle injection due to the neutral beam system. The neutral beam injection (NBI) contribution takes into account both hot and cold particle injection as well as the dependences of the full-, half-, and third-energy injected particles giving the D, D_2, and D_3 injection rates, respectively. These terms have an error (i.e., 1-σ standard deviation) estimated to be $<10\%$ for the gas puffing system and $\sim 19\%$ in the NBI calculation. $Q_{\mathrm{pump}}(t)$ is the total exhaust rate of the divertor cryopumping system where $Q_{pump}(t) = S_{\mathrm{pump}}(P) \cdot P_{\mathrm{PLENUM}}(t)$. $S_{\mathrm{pump}}(P)$ is the pressure dependent pumping speed and is typically $\sim$ 20-25 kL/s for experiments in this study. $P_{\mathrm{PLENUM}}(t)$ is the plenum pressure of the pump. The $Q_{\mathrm{pump}}(t)$ term has an estimated error of $\sim 8\%$ and is largely dominated by the uncertainty in determining $S_{\mathrm{pump}}(P)$. The three cryopumping systems in DIII-D are summed to give the total exhaust rate. In these experiments the main turbomolecular pumps are isolated from the vessel for the entire experiment and are only opened to pump-out the vessel after the cryo-pumps are warmed to liquid nitrogen temperatures ($\sim$ 80 K). It is also assumed that the NBI cryo-system pumped a negligible amount from the main chamber due to the very low neutral pressure near the NBI ducts at the midplane coupled with the relatively low effective pumping speed ($\sim$ 5.8 kL/s) of this system to the main chamber. dN_{P}/dt is the rate change in the core plasma density, $= \bar{n}_{\mathrm{e}}(t) \cdot V_{\mathrm{Plasma}}(t)$, where $\bar{n}_{\mathrm{e}}(t)$ is the line averaged density from a CO_2 interferometer and $V_{\mathrm{Plasma}}(t)$ is the plasma volume as calculated from EFIT. This term has an error $\sim 9.5\%$. Finally dN_0/dt is the rate change of the un-pumped neutral density inside the pumping plenum, $= V_{\mathrm{PLENUM}} \cdot P_{\mathrm{PLENUM}}(t)$, and has a calculated error $\sim 14\%$. Through error propagation of the RHS of Eq. 1, $\Gamma_{\mathrm{WALL}}(t)$ is determined to have a total error of $\sim$ 20-27%. This error combines both measurement and systematic error and, as will be discussed in the next paragraph, is

shown to be dominated by systematic errors in various terms on the RHS; some of which have already been discussed. Throughout the rest of this paper, this global particle balance is referred to as a dynamic balance because it gives a time history of the particle balance throughout the discharge. An example of the balance and the error in each term is given in Fig. 1(b)-1(f).

A second method of particle balance involves warming the main cryopump lines to liquid nitrogen temperatures, which releases the molecules (e.g., D_2/H_2, water and hydrocarbons, and other potential impurities) otherwise "stuck" to the surface. This process is termed "regeneration." This is done after a series of shots with the vessel isolated from all external pumping sources. The in-vessel pressure rise is measured with a highly accurate capacitance manometer (CM) gauge. The amount of gas released from the cryopump regeneration is then compared to the amount of gas injected in the series of shots, which is also determined with the CM gauge. Given that both the pressure measurement and the volume of the vessel are known to within $\leq 1\%$, this method is considered the most accurate way to determine the amount of retained fuel on a shot to shot basis. In this paper, this method is referred to as a static particle balance because it is measured after the discharge is over and thus gives a single number for the net fuel retention in the vessel surfaces during a series of discharges. This method has been used successfully on other tokamaks to give accurate measure of the retention amount [10,19].

In this study, we compare the fuel retention determined through the dynamic and static methods for discharges with the same operating conditions. The static balance method, whereby the gas retained on the cryopumps is released, is employed after every five discharges to increase the signal-to-noise on the CM gauge. We find that both methods agree to within $\sim 5\%$. It is found that impurities, i.e., non-pure hydrogenic species, do not significantly affect the D fuel retention measurements. The dynamic balance uses $\langle Z_{eff} \rangle = 2$ for the impurity content of the core plasma. This value is measured during these experiments with contributions predominately coming from the carbon PFCs [20]. RGA measurements taken during the cyropump regeneration show very small amounts of gases other than pure D_2. The main non-pure hydrogenic gases detected are water (i.e., D_2O or H_2O) at a relative partial pressure of $\sim 2\%$, and other hydrocarbon gases (e.g. methane, etc.) at a relative partial pressure of $\leq 0.1\%$.

For the studies in this paper, typical discharge parameters are: $I_p \sim 1$ MA, $\langle n_e \rangle \sim 3 \times 10^{19}$ m^{-3}, and Greenwald fractions, $f_{GW} = \langle n_e \rangle / n_{GW} \sim 0.3$ where $n_{GW} \equiv I_p[MA] / (\pi a[\mathrm{m}]^2)[\times 10^{20} \mathrm{m}^{-3}]$. The auxiliary power is from off-axis electron cyclotron heating (ECH) = 3 MW or co-current neutral beam injection = 3 MW. All discharges are upper single null with the $B \times \nabla B$ drift into the x-point leading to optimal H-mode access. The discharges are divertor cryopumped with the inner and outer strikepoint pumped independently.

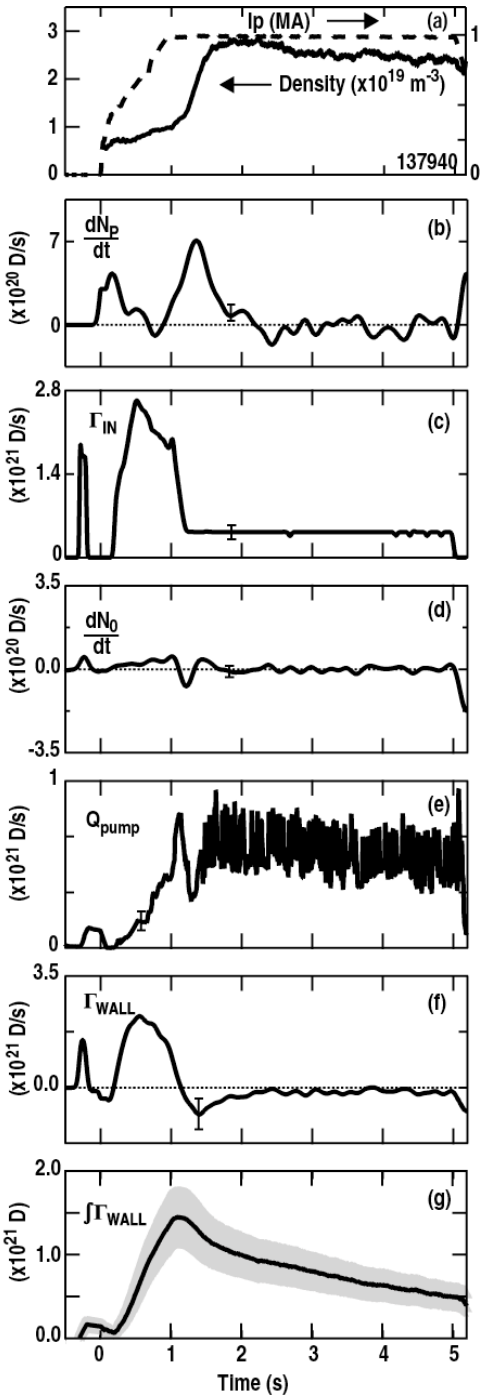

Fig. 1. An example of the dynamic particle balance on DIII-D. (a) For reference, plasma current, I_p, and density time histories where $f_{GW} = 0.27$. (b) The rate change of the core electron particle density. (c) The particle injection rate either by gas puffing, NBI, or both. (d) The rate change in the un-pumped neutrals in the cryopump plenums. (e) The total particles exhausted from the cryopumps. (f) The D retention rate. (g) The time-integral of the retention rate (the D particle inventory).

III. ANALYSIS AND RESULTS

The purpose of these experiments was to utilize both the dynamic and static particle balance methods in ELMy H-mode discharges to determine the amount of "loosely-bound" recoverable D and co-deposited D in the graphite PFCs of DIII-D. This effort is in contrast to past DIII-D fuel retention experiments which showed the cryopumps "conditioned" the walls to a degree that between shot GDC was not necessary [17,20,21]. The current experiments are also an extension of previous fuel retention on DIII-D in Ohmic-heating only discharges that investigated cryopump effects on retention. In those experiments, it was found that the cryopump did *not* affect the total D retained per shot, $\sim 10^{21}$ D / discharge, or $\sim 80\%$ of the fuel injected without cryopumping. The cyropump did, however, increase the required external fueling, thus decreasing the ratio of retention to fueling; however the cryopump apparently had no effect on the physical mechanism responsible for the strong retention [22].

Figure 1 gives the typical results of the dynamic particle balance with panels (b–f) showing the time histories of the terms in Eq. (1), with error bars for each term also shown. The L-H transition occurs at ~ 1.1 s as is evident by the increase in dN_P/dt [Fig. 1(b)] at this time, and the NBI was initiated right before the transition (at 1 s) and is evident in Q_{pump} [Fig. 1(e)] by a quick rise followed by a sharp decrease when the H-mode transition occurs. The L-H transition is also where $\Gamma_{IN}(t)$ [Fig. 1(c)] transitions from being dominated by gas puffing to NBI fueled, and the fueling rate decreases by a factor of 3. The ELMs during the H-mode period cause fast transients in Q_{pump} [Fig. 1(e)]. One salient feature of these discharges is the sharp decrease in the D retention rate after the transition to H-mode [Fig. 1(f)]. This leads to a negative D retention rate initially and then a very small net flux, effectively zero within the uncertainties, for the remainder of the discharge. The integral of the retention rate yields the calculated retention inventory in the vessel surfaces. In Fig. 1(g), it can be seen that most of the calculated retention inventory accumulates during the initial start-up phase of the discharge $(< 1.1$ s$)$, and that during the steady-state phase the inventory reduces by $\sim$ factor of 2, which is even the case to within the uncertainty of the calculation – shown as a grey band around the particle inventory. Balancing the particle injection rate with the exhaust rate within the measurement uncertainty, or in this case, even exceeding the injection rate with the exhaust is a typical result for DIII-D [17]. Recent fuel retention results from numerous other tokamaks [5,8-10,23,24] have also shown a matching of the injected flux with the exhausted particle flux when the injected particle rate is low

($f_{GW} \leq 0.7$). The results in this current experiment where $f_{GW} \sim 0.3$, support those findings.

These experiments are carried out in discharges with either NBI heating or ECH. EC-only heated discharges allow the particle balance experiment to be conducted without the extra source of neutrals from NBI, thus giving a more accurate dynamic balance by eliminating the highly uncertain NBI source term. A comparison of particle balance in an ECH versus a NBI heated discharge is show in Fig. 2 and shows that both heating methods lead to similar results. For matched discharges (i.e. density within 10%, input power, and shape), there is an increase in Γ_{IN} by feedback-controlled gas puffing [Fig. 2(b)] to maintain the same density for the ECH discharge during the steady-state portion of the discharge. This could be due to the absence of the more efficient central NBI fueling source. This gas puffing does lead to an increase in Q_{pump}, but beyond a transient increase in the fuel retention rate at $\sim$1.25-1.5 s [Fig. 2(d)], the retention inventories are similar [Fig. 2(e)].

Variation in the retention rate from discharge to discharge is a key feature of the dynamic balance analysis and leads to difficultly in predicting the total inventory on a shot-to-shot basis. This is exemplified in Fig. 3. Here, a series of identical ECH shots with the discharge input parameters held constant are taken. The shot-to-shot variability in the inventory is clear in Fig. 3(a) and is outside the estimated uncertainty in the calculation. This variability is typical for all discharges in this study. The main components of Eq. (1) are shown in Fig. 3(b)–3(d). From Fig. 3(c), the variation in Q_{pump} from $\sim$1-1.75 s gives the variation seen in Fig. 3(a). The Γ_{WALL} trace almost overlays for $t < 1$ s and there is some random variation in the time history from 1.75 s until the end of the discharge. The seemingly random variation could be due to the details and changes in the heating of the divertor targets due to ELMs and/or accumulation of analysis errors through integration.

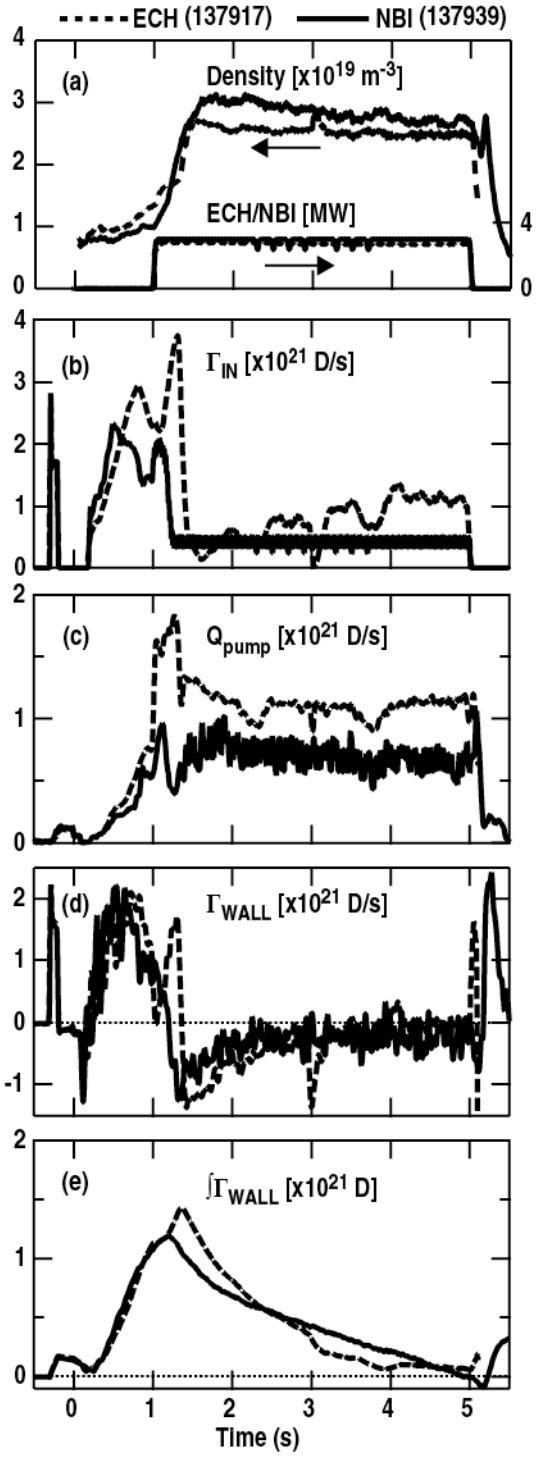

Fig. 2. A comparison of an ECH and NBI particle dynamic particle balance. (a) The line-averaged density and auxiliary power for each discharge. f_{GW} = 0.28-0.3 for the two discharges. (b) The total injected particle rate. (c) The total particle exhaust rate. (d) The D retention rate. (e) The D particle inventory.

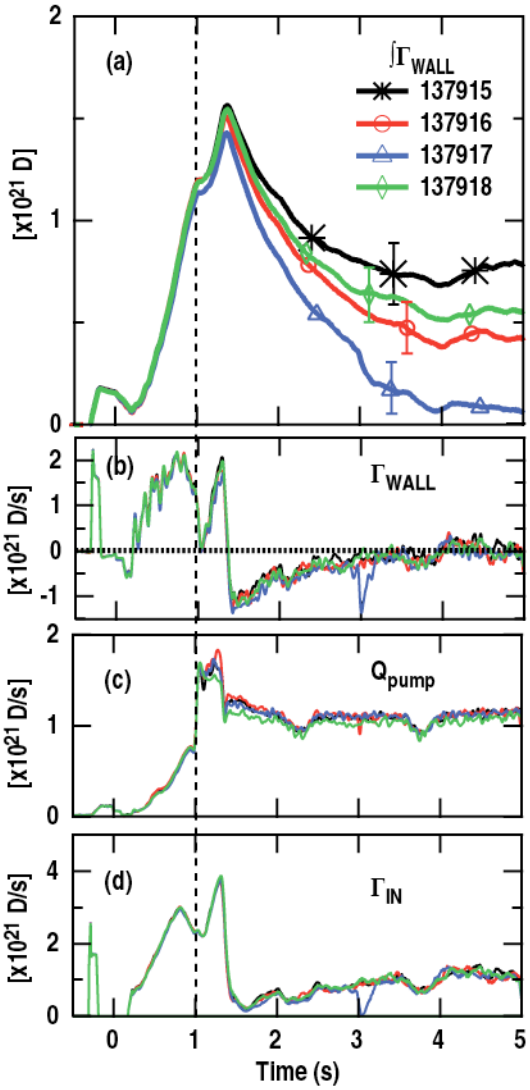

Fig. 3. A series of similar ECH ELMy H-mode discharges where the dashed vertical line marks when the ECH initiates. $f_{GW} = 0.28$ in this discharge series. (a) The particle inventory of the (4) discharges. (b) The D retention rate for the series. (c) The exhaust rate for the series. (d) The injected particle rate for the series.

The effect of ELMs on the local PFC particle content was studied on both ASDEX-U and DIII-D [25]. In that study, the fast pressure fluctuations were attributed to fast variations in the local absorption/desorption due to the ELMs and occur on time scales ~ 1 ms. Since the dynamic balance in ELMy phase of the discharge is $\Gamma_{WALL} = \Gamma_{IN} - Q_{pump}$, the variation in the magnitude of particles released by each ELM would be incorporated into the time integral of the global balance. Such variations in the ELM-driven bursts of gas could lead to a real shot-to-shot variation in the global balance as well as an increase in the statistical uncertainty of the global particle balance when ELMs are present. An example of these ELM-driven gas bursts are shown in Fig. 4. The pressure from a fast ionization gauge in the pump plenum nearest the outer strikepoint

(OSP), P_{OSP}, for an ECH discharge is shown in Fig. 4(a). Fig. 4(b) shows the OSP D_α signal, which is used as a metric for ELM events. An expanded view in time of the D_α and P_{OSP} traces around the ELM-free to ELMy period [Fig. 4(c)] shows a direct correlation between D_α and P_{OSP} not only to the L-H transition (~ 1.275 s) but also the ELM events. The exact magnitude and width of the ELM transients in P_{OSP} is variable shot-to-shot and between NBI and ECH discharges. Therefore, the effect on the global balance is hard to predict and/or characterize *a priori*.

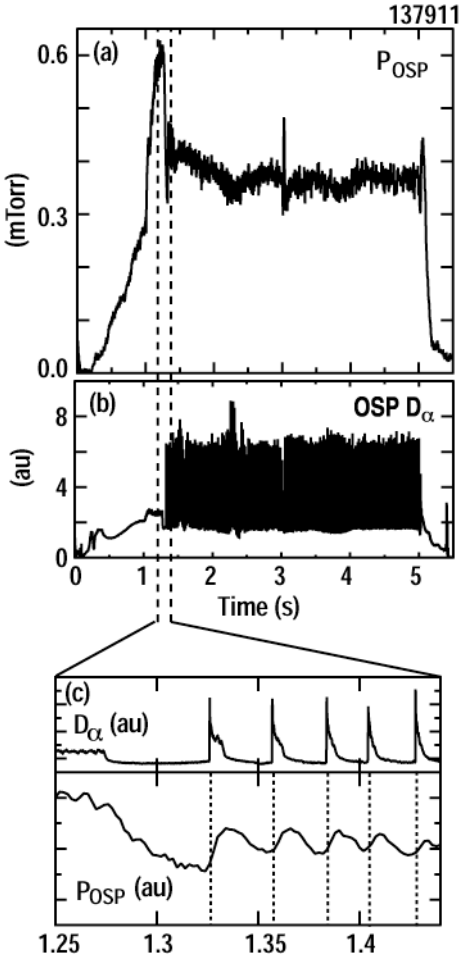

Fig. 4. Comparison of the pressure, P_{OSP}, and D_α signal during H-mode showing the effect of ELMs on the cryopump plenum pressure. (a) The time history of the P_{OSP}. (b) The time history of the OSP D_α. (c) A zoom in time of the L-H transition showing the correlation between the ELMs and pressure rise in the pump plenum.

Both particle balance methods are used to determine the amount of loosely-bound retained fuel during a single run-day on DIII-D. In this experiment, the vacuum vessel is taken to an average temperature of 350°C for 3 hours before the experiment to release a level of D from previous experiments, and after this bake the PFCs are considered free of loosely bound particles. A run-day is then performed (30 shots of ~5.5 s each) and

another vessel bake is performed while carefully measuring the total pressure rise during the bake. This second bake was truncated in time due to the logistics of the experiment, and so the vessel only reached ~ 320°C for a short duration. Therefore, the amount of D released from this truncated bake is considered an upper-bound on any further estimate of the fuel remaining in PFC surfaces. The outcome of this experiment is shown in Fig. 5, which shows the retained fuel amount for both methods as determined throughout the run-day on the left-hand side of the figure. This amount is then compared to the total amount of gas released during the vessel bake at the end of the day (right-hand side of the plot). The dynamic balance is shown as a continuous line and the static balance is represented with individual markers. The light grey bands are a 5% variation as was calculated previously as the difference between the two balance methods.

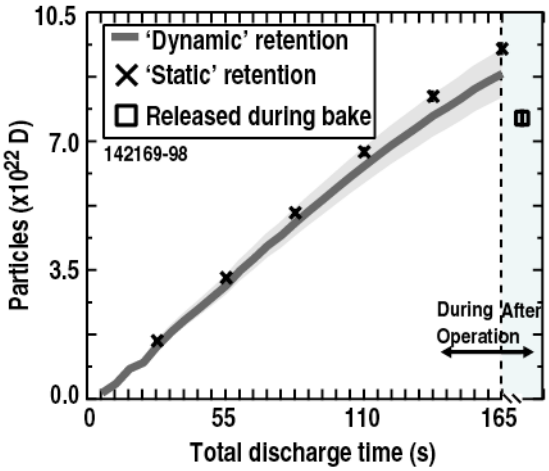

Fig. 5. A time history of the amount of retained fuel from both the dynamic and static particle balance for a complete run-day. Also shown is the amount of particles released from a vessel bake after the run-day. $f_{GW} \sim 0.27$ across this series of discharges.

From the figure, between $\sim 8.8 - 9.7 \times 10^{22}$ D is calculated to be retained (i.e., injected minus exhausted fuel) over that run-day. The average retention for this series of discharges is 5-10 times higher than the typical retention amounts determined in the previous experiments (i.e., the data shown in Figures 1-3) even though the absolute density and f_{GW} were similar -- $\langle n_e \rangle = 2.7 \times 10^{19}$ m^{-3} and $f_{GW} = 0.27$ in these experiments. The higher retention is due to feedback control issues which lead to higher gas-puffing rates to attain the same $\langle n_e \rangle$ as in previous experiments and a misalignment of the inner strikepoint to the cyropump baffling resulting in non-optimal neutral coupling to the pump plenum. Variations in the level of particle depletion from the bake prior to these series of shots could also play a role in these particular results. These particular discharges retain ~ 55% of the 1.7×10^{23} injected fuel particles. It should be noted that Fig. 5 shows no signs of the retention inventory saturated even though retained inventory has surpassed the generally accepted saturation level of $\sim 1 \times 10^{21} \text{m}^{-2}$; given

that DIII-D has a graphite surface area of $\sim 70\ m^{-2}$. Nonetheless, the bake releases $\sim 7.3 - 7.7 \times 10^{22}$ particles, i.e. $\sim 80\%$ of the retained D, and, most interestingly, this is the amount of particles needed to equal the $\sim 1 \times 10^{21} m^{-2}$ saturation level. In the end, $\sim 10 - 20 \times 10^{21}$ D particles are still retained after baking.

In an effort to show the differences in the net inventory between Fig. 5 and Figs. 1-4, a histogram of the database of all the particle balance experiments in this study has been made. Fig. 6(a) shows a histogram of the ending total inventory ($\int \Gamma_{WALL}$ at ~ 5 s) for all discharges. As can be seen, there are two peaks in the histogram; one at $\sim 0.8 \times 10^{21}$ D which is the data from discharges similar to those shown in Figs. 1-4. The other peak is $\sim 2.5 \times 10^{21}$ D and is from discharges in Fig. 5 where feedback control was not optimal. Therefore unless feedback control is lost the average global retention fluence on DIII-D is found to be $\sim 1.11 \times 10^{19} m^{-2}$. It should be repeated that the initial wall conditions of these discharges are mostly depleted. Therefore the results differ from the early global particle balance experiments done on DIII-D where walls were intentionally loaded within a run-day [17].

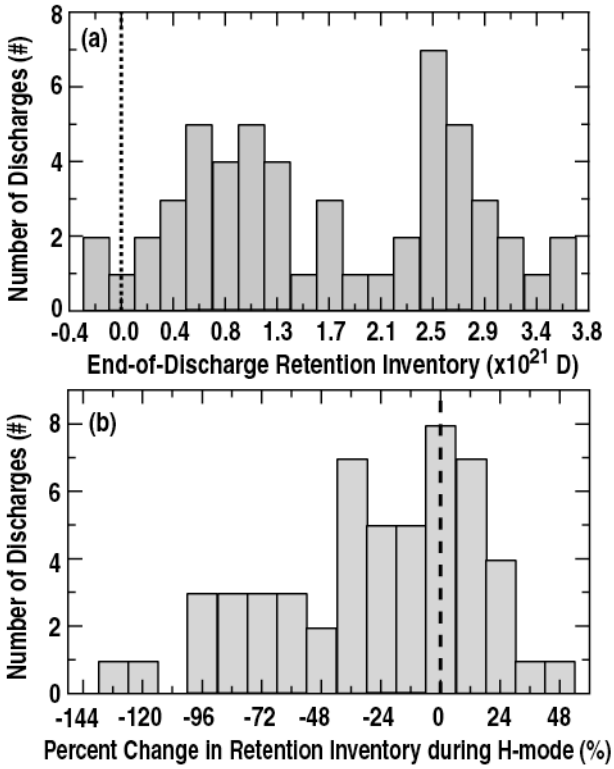

Fig. 6. (a) A histogram of the End-of-Discharge retention inventory for all the discharges in the experiments of this study. (b) A histogram of the percent change in the retention inventory during the H-mode phase of the same database.

Nonetheless given the same database, a clear trend is seen that during the H-mode phase there is almost always a decrease or no change in the retention inventory. Fig. 6(b) shows a histogram of the percent change in the retention inventory during the steady-state H-mode phase of this discharges. The shots that do have increased H-mode inventory in this data set are those with the highest end-of-discharge inventory shown in Fig. 6(a) where there is limited feedback control. It is very clear that at $f_{GW} \sim 0.3$ and with strong divertor cryopumping there is almost always a decrease in the retention inventory.

Finally, the global particle balance is applied to resonant magnetic perturbation (RMP) ELM suppressed discharges which is part of an effort to determine the effects of wall pumping on the density reduction due to this applied 3-D magnetic perturbation [26]. Figure 7 shows a comparison of an RMP discharge to one of the NBI heated discharges preformed in this study. The RMP discharge is typical for recent ELM-suppression experiments which are carried out on different run-days with different beginning wall conditions [27]. Fig. 7(a) gives the line-averaged density for the discharges. The RMP time history shows the characteristic of "density pumpout", which occurs at ~ 2 s. ELM suppression is seen in the D_α time history shown in Fig. 7(c). After the density pumpout at 2 s the two discharges have similar $\langle n_e \rangle (\sim 2 \times 10^{19} \mathrm{m}^{-3})$ and $\beta_N (\sim 1.7)$. Qualitatively from Fig. 7(g), the time histories of the retention inventory are similar between the two discharges in the stationary phase, with the retained fluxes are near zero, even though the RMP total retention inventory [Fig. 7(h)] is ~ 3-4 times higher before the steady-state phase and much higher at the end of the discharge. The higher retention inventory in the RMP discharge compared to the non-RMP discharge is due to the large Γ_{IN} in the initial phase of the RMP case where Γ_{IN} was on average 4 times higher [Fig. 7(e)]. One of the characteristics of these RMP discharges is that particle exhaust to the cryopumping system increases when the perturbation is applied. This is shown in Fig. 7(f) where the exhaust rate is similar up to 2 s (i.e., before the RMP is applied) after which this rate in the RMP discharge increases by $\sim 30\%$. As the strikepoint is perturbed by the RMP, the magnetic geometry of the divertor is changed. Ultimately, this change in the divertor topology leads to changes in the exhaust rate of the cryopump. Nonetheless, the increase in pumping does not decrease the calculated retention inventory accumulated in the initial phase as opposed to the non-RMP discharge where the retention inventory decreases significantly in the steady-state phase. On the other hand, it does maintain a constant retention inventory (i.e., no wall uptake) throughout the RMP phase, which is most likely due to the reduced particle confinement (i.e., density pumpout).

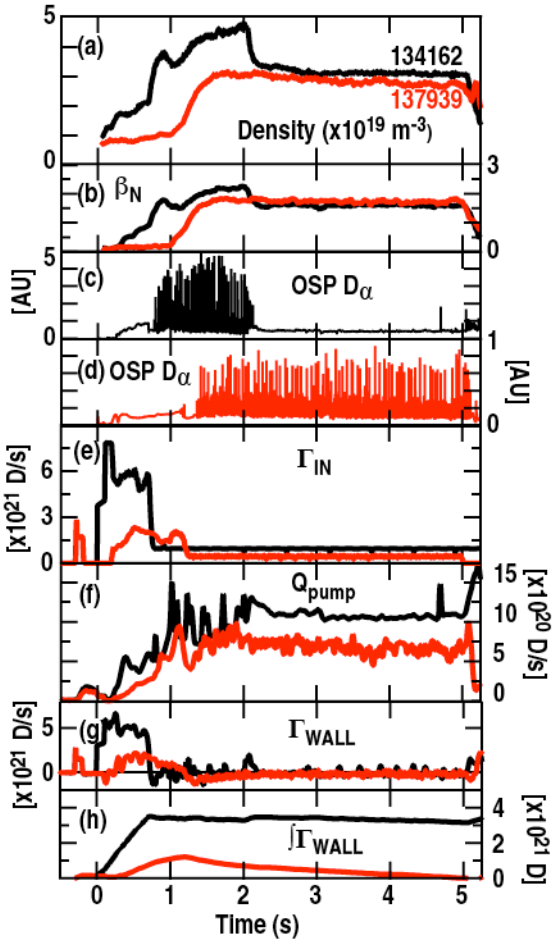

Fig. 7. A comparison of a typical ELMy H-mode discharge and a typical RMP ELM-suppressed discharge. (a) The line averaged electron density for both discharges —notice the density pumpout when the RMP is applied at ~ 2.0 s. (b) and (c) are the OSP D_α for each discharge — again the ELM suppression is apparent in (b) at ~ 2 s. (e) The total injected particle rate for both discharges. (f) The total exhaust rate for each discharge. (g) The retention rate for each discharge. (h) The D retention inventory for each discharge.

IV. DISCUSSION

The experiments reported here add to the database of similar results from other devices that have addressed particle balance. Namely, at low core density (i.e., low fueling rates) and with strong divertor pumping, the steady-state phase of the discharge can exhibit no net fuel retention within the experimental uncertainty. There are several explanations for such behavior: a) the implantation has saturated and/or; b) the co-deposition rates are so low during the stationary phase of the discharge that net retention cannot be measured and/or; c) some release mechanisms from the PFCs match retention (co-deposition) elsewhere. These observations are independent of heating method since we completed experiments with similar properties using both ECH and NBI heating. The implication is that the tightly-bound (i.e., long-term) fuel retention from co-deposition is within the uncertainty of this type of calculation and therefore the dynamic particle balance does not have the accuracy to reliably determine the D co-deposition. Furthermore, the explanation as to why the retention rate changes from a high value in the initial phase of the discharge to near zero in the steady-state phase is unknown at this point. Models that depend on poloidally varying ion and neutral fluxes to the walls have been suggested which would then give a complex variety of wall saturation times (from 0.1-100 seconds) depending on the phase of the discharge [28,29]. These models qualitatively agree with experimental data for DIII-D, Tore Supra [4], and JT-60U [28], but have yet to be quantitatively compared to experiments.

When the retention rate found in the previous section is normalized to the measured ion flux to the divertor targets, $\Gamma_{D+} \sim 4\times10^{23}$ D/s, it is found to be $\sim 0.25\%$ which is lower than the $\sim 1\%$ reported in metal PFCs [10], but is within a factor of 2 of that reported on Ohmic discharges in DIII-D [22]. The ion fluxes are measured in both experiments (Ohmic and ELMy H-mode) during the steady-state phase of the discharges, and the normalized quantities seem to suggest a common retention mechanism. Although it should be pointed out that the flux needed to saturate the wall in DIII-D ($\sim 1\times10^{17}\,\mathrm{m^{-2}s^{-1}}$) is well below this measured flux. The divertor conditions in these low core density ($f_{GW} \sim 0.3$) studies are in the high recycling regime.

The results given in the previous section allow us to make a reasonable estimate of the co-deposition rate occurring in DIII-D and compare this to the current understanding of D concentrations in these layers. The co-deposition rate can take the following simple form; $\Gamma_{\mathrm{CoDep}} = \Gamma_C \cdot (D/C)$ where Γ_C is the net carbon erosion/re-deposition rate and D/C is the deuterium concentration in the co-deposition layer [4]. In the previous section, it was determined that $\sim 1-2\times10^{22}$ D atoms have been retained even after a limited

baking of the tiles. Given the following assumptions: a) that this retention is due entirely to co-deposition and; b) that the co-deposition is occurring at roughly an equal rate throughout the whole discharge, which may or may not be true, one gets a co-deposition rate, $\Gamma_{CoDep} = 0.6 - 1.2 \times 10^{20}$ D/s based on Fig. 5. It is worth repeating that this is a conservatively high estimate of the co-deposition rate because of the limited bake used in the determining the final retention amount. Finally, using the above Γ_{CoDep} and an estimate of $\Gamma_C = 1.9 \times 10^{20}$ C/s based on past work on carbon erosion in DIII-D [30], one would get a globally averaged D/C ~ 0.3-0.6 which is well within the estimates on DIII-D and other studies [31-33].

V. CONCLUSIONS

The finding that most of the fuel retention occurs in the initial phase of the discharge is consistent with most other tokamaks that have performed global particle balances experiments in a pumped divertor configuration [5,8,23,24]. The dominance of external pumping occurs in the operating regime where low external fueling is needed to maintain a steady density with $f_{GW} <\sim 0.7$ from previous studies. Under these conditions, the divertor is most likely in a high recycling state and ELM interactions with the targets can affect the retention properties. On the other hand, the previous studies cited showed that when $f_{GW} >\sim 0.7$ which will be the case in future burning plasma experiments, strong external fueling is necessary to maintain the density and the divertor will most likely be in a detached state where the high density and low temperatures could alter the fuel retention mechanisms through changes in the chemical and physical wall sputtering rates. It is also implied from the global particle balance that ELM control via RMP does not strongly increase the fuel retention rate in the steady-state phase of the discharge when compared to ELMy H-mode retention.

Another encouraging result is that a large fraction of the estimated injected fuel is released by a simple bake of the vessel. This is assumed to be the loosely bound fuel where the small fraction of tightly bound fuel (i.e., trapped by co-deposition or deep implantation) would have to be removed by some other method.

The exact retention mechanism and the most effected region of the vessel (i.e., divertor versus main chamber) for the seemingly dependence on particle source strength and/or divertor transport properties has not been determined. This would suggest further research on how wall retention depends on fueling source type, plasma core conditions, poloidal distribution of ion/neutral wall fluxes, and/or divertor conditions.

REFERENCES

[1] B. Lipschultz, *et al.*, Nucl. Fusion **47**, 1189 (2007).

[2] A. Loarte, *et al.*, Nucl. Fusion **47**, S203 (2007).

[3] J. Roth, *et al.*, J. Nucl. Mater. **390-391**, 1 (2009).

[4] E. Tsitrone, *et al.*, J. Nucl. Mater. **363**, 12 (2007).

[5] T. Loarer, *et al.*, J. Nucl. Mater. **390-391**, 20 (2009).

[6] T. Loarer, *et al.*, Nucl. Fusion **47**, 1112 (2007).

[7] V. Philipps, *et al.*, Plasma Phys. Control. Fusion **45**, A17 (2003).

[8] T. Nakano, *et al.*, Nucl. Fusion **48**, 085002 (2008).

[9] V. Rohde, *et al.*, Nucl. Fusion **49**, 085031 (2009).

[10] B. Lipschultz, *et al.*, Nucl. Fusion **49**, 045009 (2009).

[11] W. Möller, *et al.*, J. Nucl. Mater. **162-164**, 138 (1989).

[12] G. Federici, *et al.*, Nucl. Fusion **41**, 1967 (2001).

[13] J.W. Davis and A.A. Haasz, J. Nucl. Mater. **390-391**, 532 (2009).

[14] D.G. Whyte and J.W. Davis, J. Nucl. Mater. **337**, 560 (2005).

[15] H. Kubo, *et al.*, "Particle Control Under Wall Saturation in Long-pulse High Density H-mode Plasmas of JT-60," Proc. of 21st Int. Conf. on Fusion Energy (Chandu, China 2006); http://www-naweb.iaea.org/napc/physics/FEC/FEC2006/ html/ index.htm.

[16] E. Tsitrone, *et al.*, Plasma Phys. Control. Fusion **44**, 701 (2002).

[17] R. Maingi, *et al.*, Nucl. Fusion **36**, 245 (1996).

[18] T. Loarer, *et al.*, "Overview of Gas Balance in Plasma Fusion Devices," Proc. of 20th Int. Conf. on Fusion Energy (Villamoura, Portugal 2004); http://www-naweb.iaea.org/napc/physics/FEC/FEC2004/datasets/index.html.

[19] V. Philipps, *et al.*, J. Nucl. Mater. **390-391**, 478 (2009).

[20] M.A. Mahdavi, *et al.*, Proc. of 20th Euro. Conf. on Control. Fusion and Plasma Physics, Lison 1993 (European Physical Society, Petit-Lancy 1993) Vol. 17C, p. 647.

[21] S.L. Allen, *et al.*, Plasma Phys. Control. Fusion **37**, A191 (1995).

[22] W.P. West *et al.*, "Gas balance in Ohmic discharges on DIII-D," Bulletin of the American Physical Society, 50th APS-DPP Meeting (Dallas, TX), http://meetings.aps.org/link/BAPS.2008.DPP.JP6.63.

[23] N. Asakura, *et al.*, Plasma Phys. Control. Fusion **46**, B335 (2004).

[24] T. Nakano, *et al.*, J. Nucl. Mater. **363-365**, 1315 (2007).

[25] G. Haas, *et al.*, J. Nucl. Mater. **266-269**, 1065 (1999).

[26] E.A. Unterberg, *et al.*, Nucl. Fusion **50**, 034011 (2010).

[27] T.E. Evans, *et al.*, Nucl. Fusion **48**, 024002 (2008).

[28] H. Takenaga, *et al.*, Nucl. Fusion **46**, S39 (2006).

[29] P.K. Mioduszewski and L.W. Owen, J. Nucl. Mater. **290-293**, 443 (2001).

[30] D.G. Whyte, *et al.*, Nucl. Fusion **38**, 387 (1997).

[31] D.G. Whyte, *et al.*, J. Nucl. Mater. **266-269**, 67 (1999).

[32] K. Maski, *et al.*, Nucl. Fusion **47**, 1577 (2007).

[33] J.P. Coed, *et al.*, J. Nucl. Mater. **290-293**, 224 (2001).

ACKNOWLEDGMENTS

This work was supported by the U.S. Department of Energy under DE-AC05-00OR22725, DE-AC52-07NA27344, DE-FC02-04ER54698, DE-AC04-94AL85000, and DE-FG02-04ER54762. EAU would like to acknowledge the fruitful discussions and encouragement from M.A. Mahdavi and P.C. Stangeby. He would also like to recognize the initial encouragement and development of this work on DIII-D by the late W.P. West.